

Three Zr(IV)-Substituted Polyoxotungstate Aggregates: Structural Transformation from Tungstoantimonate to Tungstophosphate Induced by pH

Hai-Lou Li, Chen Lian, Da-Peng Yin, and Guo-Yu Yang*

Cite This: <https://dx.doi.org/10.1021/acs.inorgchem.0c01910>

Read Online

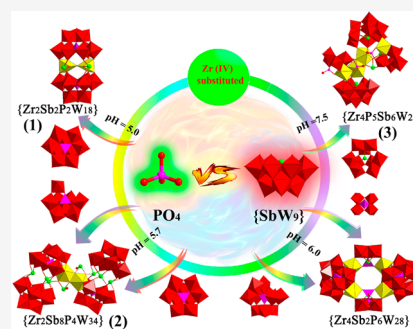
ACCESS |

Metrics & More

Article Recommendations

Supporting Information

ABSTRACT: Three novel Zr-substituted polyoxotungstate aggregates $[\text{H}_2\text{N}(\text{CH}_3)_2]_7\text{NaH}_2[\text{Zr}_2\text{Sb}_2\text{O}_3(\text{A-}\alpha\text{-PW}_9\text{O}_{34})_2]\cdot 16\text{H}_2\text{O}$ (**1**), $[\text{H}_2\text{N}(\text{CH}_3)_2]_6\text{H}_{12}[\text{ZrSb}_4(\text{OH})\text{O}_2(\text{A-}\alpha\text{-PW}_8\text{O}_{32})(\text{A-}\alpha\text{-PW}_9\text{O}_{34})]_2\cdot 33\text{H}_2\text{O}$ (**2**), and $[\text{H}_2\text{N}(\text{CH}_3)_2]_4\text{Na}_{11.5}\text{H}_{4.5}[\text{Zr}_4\text{W}_8\text{Sb}_4\text{P}_5\text{O}_{49}(\text{OH})_5(\text{B-}\alpha\text{-SbW}_9\text{O}_{33})_2]\cdot 53\text{H}_2\text{O}$ (**3**) have been made in hydrothermal reactions of the $[\text{B-}\alpha\text{-SbW}_9\text{O}_{33}]^{9-}$ precursor with Zr^{4+} cations and PO_4^{3-} anions in the presence of dimethylamine hydrochloride and sodium acetate buffer (pH = 4.8) and structurally characterized. Different pH values induce structural transformation from tungstoantimonate (TA) to tungstophosphate (TP). **1** is a di-Zr-substituted sandwich-type TP, the tetranuclear heterometallic $[\text{Zr}_2\text{Sb}_2\text{O}_3]^{8+}$ entity sandwiched by two $[\text{A-}\alpha\text{-PW}_9\text{O}_{34}]^{9-}$ moieties. **2** is a double sandwich-type structure, which can be perceived as two equivalent sandwiched $[\text{Sb}_3(\text{PW}_8\text{O}_{32})(\text{PW}_9\text{O}_{34})]^{11-}$ further sandwiching one $[\text{Sb}_2\text{Zr}_2(\text{OH})_2\text{O}_4]^{4+}$ core to form a novel large-size sandwich-type architecture. Different from **1** and **2**, **3** is a tetra-Zr-substituted sandwiched configuration, in which two $[\text{B-}\alpha\text{-SbW}_9\text{O}_{33}]^{9-}$ fragments sandwich a unique 21-core Sb–P–W–Zr oxo cluster ($\{\text{Zr}_4\text{W}_8\text{Sb}_4\text{P}_5\}$). Furthermore, the catalytic oxidation of aromatic thioethers by **3** as the heterogeneous catalyst has been investigated, showing high conversion and remarkable selectivity as well as excellent recyclability.



INTRODUCTION

The polyoxometalates (POMs), a well-known large class of metal-oxo clusters, has existed for nearly two hundred years.^{1–5} Great efforts have been devoted to POMs and led to a rapid growth due to their structural diversity and extensive applications in various fields, such as magnetism, catalysis, medicine, and photophysics.^{6–11} In POMs, two important subfamilies of tungstoantimonates (TAs) and tungstophosphates (TPs) with unique structures and excellent properties have attracted a lot of attention in the past decades, especially the functionalization, such as catalytic and magnetic properties, by transition metal (TM) ingredients, resulting in many TM-containing TAs and TPs having been made.^{12–20} Nevertheless, although Zr-substituted polyoxotungstates (POTs) possess good catalytic performance,^{21,22} only a few reports have been covered so far.^{23–27}

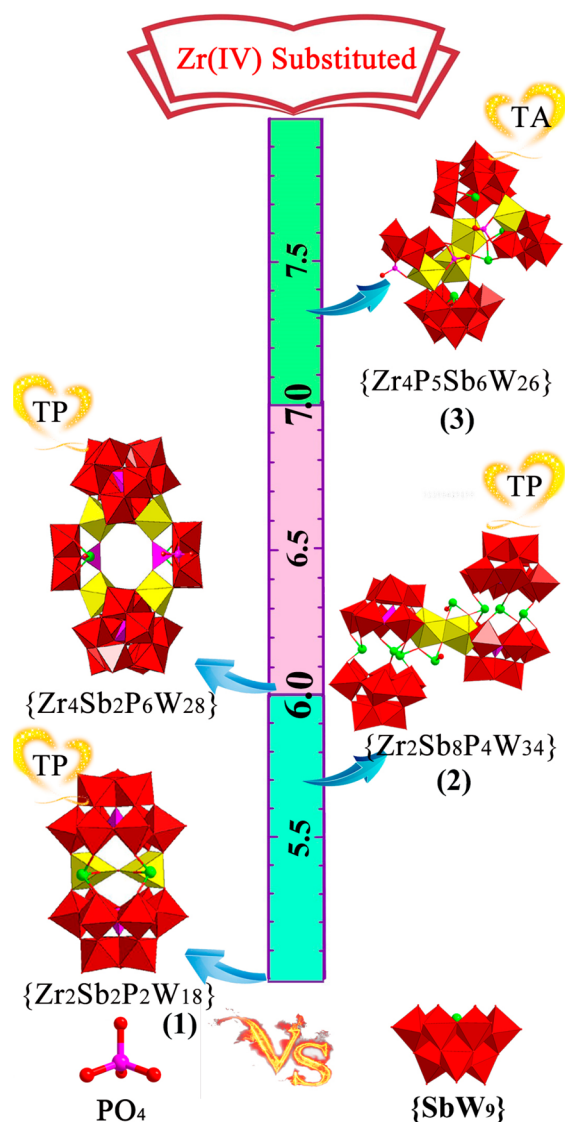
The vacant Keggin precursor linked functional units (such as TMs, lanthanides, organometallic entities)^{28–31} represents one of the largest and most active candidates widely used for making novel POT architectures. There have been a few studies on the conversion between two types of precursors;^{32–35} however, more possibilities to generate new building blocks and obtain heteroatom bridged structures during the course of transformation exist.

Recently, a novel Zr-substituted TA, $[\text{H}_2\text{N}(\text{CH}_3)_2]_7\text{Na}_3\text{H}_5[\text{Zr}_3(\text{OAc})\text{W}_7(\text{H}_2\text{O})\text{O}_{25}][\text{B-}\alpha\text{-SbW}_9\text{O}_{33}]_2\cdot 22\text{H}_2\text{O}$,³⁶ has been reported, and then by introducing PO_4^{3-} ion, a new TP

product, $[\text{H}_2\text{N}(\text{CH}_3)_2]_6\text{Na}_6\text{H}_8\{\text{Zr}_2[\text{SbP}_2\text{W}_4(\text{OH})_2\text{O}_{21}][\alpha\text{-PW}_{10}\text{O}_{38}]_2\}\cdot 50\text{H}_2\text{O}$,³⁷ has been obtained under the weak acidic conditions, in which the conversion from TA to TP was observed. On the basis of the occurrence of this configuration transformation and considering that the pH value is always a vital factor in making POMs as part of our ongoing synthesis work, we attempt to explore whether the pH affects the configuration transformation between TA and TP by elaborately regulating the pH in the subsequent experiments. Fortunately, three types of Zr-containing POTs $[\text{H}_2\text{N}(\text{CH}_3)_2]_7\text{NaH}_2[\text{Zr}_2\text{Sb}_2\text{O}_3(\text{A-}\alpha\text{-PW}_9\text{O}_{34})_2]\cdot 16\text{H}_2\text{O}$ (**1**), $[\text{H}_2\text{N}(\text{CH}_3)_2]_6\text{H}_{12}[\text{ZrSb}_4(\text{OH})\text{O}_2(\text{A-}\alpha\text{-PW}_8\text{O}_{32})(\text{A-}\alpha\text{-PW}_9\text{O}_{34})]_2\cdot 33\text{H}_2\text{O}$ (**2**), and $[\text{H}_2\text{N}(\text{CH}_3)_2]_4\text{Na}_{11.5}\text{H}_{4.5}[\text{Zr}_4\text{W}_8\text{Sb}_4\text{P}_5\text{O}_{49}(\text{OH})_5(\text{B-}\alpha\text{-SbW}_9\text{O}_{33})_2]\cdot 53\text{H}_2\text{O}$ (**3**, Scheme 1) have been made. **1** is a di-Zr-substituted TP dimer built by two $[\text{A-}\alpha\text{-PW}_9\text{O}_{34}]^{9-}$ ($\{\text{PW}_9\}$) fragments encapsulating a $\{\text{Zr}_2\text{Sb}_2\}$ ($[\text{Zr}_2\text{Sb}_2\text{O}_3]^{8+}$) core. **2** is a double sandwich-type TP, in which two equivalent sandwiched subunits $[\text{Sb}_3(\text{PW}_8\text{O}_{32})(\text{PW}_9\text{O}_{34})]^{11-}$ are further sandwiched by a $[\text{Sb}_2\text{Zr}_2(\text{OH})_2\text{O}_4]^{4+}$ core. Different from **1** and **2**, **3** is a

Received: June 28, 2020

Scheme 1. Schematic Synthetic Processes of Clusters 1, 2, 3, and 4 ($\{Zr_2[SbP_2W_4(OH)_2O_{21}][\alpha_2-PW_{10}O_{38}]\}_2\}^{37-}$)^a



^aColor codes: WO_6 octahedra, red; ZrO_x polyhedra, yellow; PO_4 tetrahedra, pink; Sb atoms, bright green; O atoms, red.

tetra-Zr-substituted sandwiched TA, showing two $[B-\alpha-SbW_9O_{33}]^{9-}$ ($\{SbW_9\}$) fragments sandwiching a unique 21-core Sb–P–W–Zr oxo cluster $[Zr_4W_8Sb_4P_5O_{49}(OH)_5]^{2-}$ ($\{Zr_4W_8Sb_4P_5\}$). Notably, during the synthesis process, we find that, under weak acid or acidic conditions, TA is easily converted to TP, whereas under neutral or alkaline conditions, this conversion is relatively difficult; it may be perceived that, under weak acid or acidic conditions, the binding of PO_4 and W-oxide units to polymerize into TP is more efficient than that of SbO_3 and W-oxide units to obtain TA, while this combined capacity is flattened under neutral and alkaline conditions. Thus, the conversion is not completed, and it only aggregates into TA. This discovery may furnish an important reference for future synthesis. Furthermore, the catalytic oxidation of thioethers by 3 as the heterogeneous catalyst has been investigated in detail, showing high conversion and prominent selectivity in the catalytic oxidation with H_2O_2 as well as good stability and excellent recyclability.

EXPERIMENTAL SECTION

Preparation of $[H_2N(CH_3)_2]_7NaH_2[Zr_7Sb_2O_3(A-\alpha-PW_9O_{34})_2] \cdot 16H_2O$ (1). $Na_9[B-\alpha-SbW_9O_{33}] \cdot 19.5H_2O$ (1.205 g, 0.421 mmol), Na_2CO_3 (0.201 g, 1.896 mmol), $Na_3PO_4 \cdot 12H_2O$ (0.501 g, 1.317 mmol), dimethylamine hydrochloride (0.402 g, 4.930 mmol), and $ZrOCl_2 \cdot 8H_2O$ (0.256 g, 0.794 mmol) were dissolved in 10 mL of 0.5 mol·L⁻¹ sodium acetate buffer (pH = 4.8). While stirring for 10 min, the pH of the solution was adjusted to 5.0 by using HCl (4 mol·L⁻¹), and after another 10 min, it was readjusted to 5.0. Then, the mixture was sealed in a 25 mL Teflon-lined bomb at 120 °C for 5 days, cooled to room temperature, and filtered. Evaporation of the solvent at room temperature resulted in faint yellow quadrangular prism crystals of 1 after several days. Yield: 82 mg (7.01% based on $Na_9[B-\alpha-SbW_9O_{33}] \cdot 19.5H_2O$).

Preparation of $[H_2N(CH_3)_2]_6H_{12}[ZrSb_4(OH)O_2(A-\alpha-PW_8O_{32})(A-\alpha-PW_9O_{34})] \cdot 33H_2O$ (2). $Na_9[B-\alpha-SbW_9O_{33}] \cdot 19.5H_2O$ (1.401 g, 0.489 mmol), Na_2CO_3 (0.198 g, 1.868 mmol), $Na_3PO_4 \cdot 12H_2O$ (0.504 g, 1.326 mmol), dimethylamine hydrochloride (0.401 g, 4.920 mmol), and $ZrOCl_2 \cdot 8H_2O$ (0.252 g, 0.782 mmol), were dissolved in 10 mL of 0.5 mol·L⁻¹ sodium acetate buffer (pH = 4.8). The following synthesis process was similar to 1, except for keeping the pH of the solution at 5.7, yielding yellow strip crystals of 2. Yield: 74 mg (5.70% based on $Na_9[B-\alpha-SbW_9O_{33}] \cdot 19.5H_2O$).

Preparation of $[H_2N(CH_3)_2]_4Na_{11.5}H_{4.5}[Zr_4W_8Sb_4P_5O_{49}(OH)_5(B-\alpha-SbW_9O_{33})_2] \cdot 53H_2O$ (3). $Na_9[B-\alpha-SbW_9O_{33}] \cdot 19.5H_2O$ (1.703 g, 0.595 mmol), Na_2CO_3 (0.405 g, 3.821 mmol), $Na_3PO_4 \cdot 12H_2O$ (0.496 g, 1.310 mmol), dimethylamine hydrochloride (0.398 g, 4.881 mmol), and $ZrOCl_2 \cdot 8H_2O$ (0.258 g, 0.801 mmol) were dissolved in 10 mL of 0.5 mol·L⁻¹ sodium acetate buffer (pH = 4.8). When the pH was kept at 7.5 by the introduction of HCl (4 mol·L⁻¹) during stirring, the mixture was sealed in a 25 mL Teflon-lined bomb at 100 °C for 5 days, then cooled to room temperature, and filtered. Evaporation of the solvent at room temperature resulted in colorless strip crystals of 3 after several days. Yield: 217 mg (11.57% based on $ZrOCl_2 \cdot 8H_2O$).

RESULTS AND DISCUSSION

Synthesis. With our continuous work on the conversion between TA and TP configurations to make novel Zr-containing POT aggregates, 1, 2, and 3 were all made by reacting $Na_3PO_4 \cdot 12H_2O$, $\{SbW_9\}$, Na_2CO_3 , and dimethylamine hydrochloride with $ZrOCl_2 \cdot 8H_2O$ under the weak acidic or neutral conditions by hydrothermal synthesis. During the course of the exploration, we gave priority to the influence of pH under similar conditions; when in different intervals, unexpectedly, several types of structures were obtained. These results of the parallel experiments revealed that pH played a crucial role in the reaction process. As pH ranges from 4.8 to 5.2, 1 was found and with the highest yield at pH 5.0. However, when pH varied from 5.3 to 5.8, 2 was obtained, and the most advantageous pH was at 5.7. Interestingly, at pH 5.7, the mixed phase of 2 and 4 ($\{Zr_2[SbP_2W_4(OH)_2O_{21}][\alpha_2-PW_{10}O_{38}]\}_2\}^{37-}$) appeared (the colors of crystals 2 and 4 were yellow and colorless, respectively; therefore, they could be mechanically separated and identified by powder X-ray diffraction patterns). Besides, experimental results indicated that pH in the range of 5.6–6.2 was all beneficial for the formation of 4, and the yield and purity were the highest when the value was close to 6.0 while keeping the other conditions unchanged. Moreover, no crystals were achieved if pH was distributed between 6.3 and 7.0. However, 3 was available at pH 7.0–7.8, and the highest yield was at pH 7.5, which was Zr-substituted TA.

Otherwise, under the optimal pH, we also paid attention to the influences of the usage amount of raw materials and reaction temperature on the products as well. We found that 1,

Table 1. Crystallographic Data and Structure Refinements for 1–3

	1	2	3
formula	C ₁₄ H ₉₀ N ₇ NaO ₈₇ P ₂ Sb ₂ W ₁₈ Zr ₂	C ₁₂ H ₁₁₈ N ₆ O ₁₇₁ P ₄ Sb ₈ W ₃₄ Zr ₂	C ₈ H _{147.5} N ₄ Na _{11.5} O ₁₇₃ P ₃ Sb ₆ W ₂₆ Zr ₄
F _w	5569.10	10624.42	9363.51
crystal system	triclinic	monoclinic	triclinic
space group	P $\bar{1}$	P2 ₁ /n	P $\bar{1}$
a, Å	13.5951(5)	26.3763(12)	21.2608(5)
b, Å	17.9815(7)	13.6682(5)	26.4779(7)
c, Å	21.8864(7)	28.3444(16)	37.4815(9)
α, deg	74.320(3)	90	98.953(2)
β, deg	75.362(3)	101.175(5)	95.250(2)
γ, deg	69.381(3)	90	111.103(2)
V, Å ⁻³	4747.0(3)	10024.9(8)	19194.2(8)
Z	2	2	4
μ, mm ⁻¹	22.629	20.705	16.723
F(000)	4948	9348	16796
T, K	293(2)	293(2)	293(2)
limiting indices	-16 ≤ h ≤ 16 -21 ≤ k ≤ 21 -26 ≤ l ≤ 25	-30 ≤ h ≤ 31 -15 ≤ k ≤ 16 -33 ≤ l ≤ 33	-25 ≤ h ≤ 25 -30 ≤ k ≤ 31 -44 ≤ l ≤ 44
no. of reflns collected	49802	94273	189254
no. of indep reflns	16685	17576	67382
R _{int}	0.0585	0.1015	0.0971
data/restraints/params	16685/15/1030	17576/30/947	67382/391/3649
GOF on F ²	1.003	1.062	1.021
final R indices [I > 2σ(I)]	R ₁ = 0.0428 wR ₂ = 0.0824	R ₁ = 0.0592 wR ₂ = 0.1363	R ₁ = 0.0723 wR ₂ = 0.1608
R indices (all data)	R ₁ = 0.0782 wR ₂ = 0.0912	R ₁ = 0.1091 wR ₂ = 0.1580	R ₁ = 0.1519 wR ₂ = 0.1961

2, and 3 could be obtained with the amount of {SbW₉} ranging from 1.200 to 1.800 g. Besides, when the usage of ZrOCl₂·8H₂O changed from 0.200 to 0.300 g, 1, 2, and 3 could be afforded, and the yields were the highest with the usage of about 0.250 g. If the dosage of Zr⁴⁺ cations was overused (>0.400 g), it was easy to get jelly. Conversely, once the amount of Zr⁴⁺ cations was too small (<0.100 g), it was difficult to obtain crystals. Finally, the temperatures between 100 and 130 °C were helpful for the formation of 1 and 2, with the most suitable temperature being 120 °C. Different from 1 and 2, the temperatures conducive to the formation of 3 were 80 to 120 °C, and the most suitable temperature was 100 °C.

Structure Description. Single-crystal X-ray diffraction shows that 1 crystallizes in triclinic space group P $\bar{1}$ (Table 1) and consists of a sandwiched polyoxoanion [Zr₂Sb₂O₃(A-α-PW₉O₃₄)₂]¹⁰⁻ ({Zr₂Sb₂}@{PW₉}₂), Figure 1a). Bond valence sum (BVS) calculations³⁸ of 1 indicate that the oxidation states of all the W, P, Sb, and Zr centers are +6, +5, +3, and +4, respectively (Table S1). The polyoxoanion is a sandwiched TP, in which a U-shaped tetranuclear {Zr₂Sb₂} unit (Figure 1b) bridges two {PW₉} fragments (Figure 1c) by -O-Sb-O-/-O-Zr-O- linkers. In the {Zr₂Sb₂} entity, two independent Zr⁴⁺ cations with the slightly distorted hexa-coordinate triangular prism geometry (Figure 1d) are defined by 4 μ-O atoms from 2 {PW₉} fragments, 1 μ-O atom of a SbO₃, and 1 μ-O atom of a ZrO₆. In addition, each SbO₃ group links to 2 {PW₉} fragments and 1 ZrO₆. Notice that the tetranuclear {Zr₂Sb₂} acting as a bridge to link two {PW₉} fragments has not been observed in POM chemistry.

Meaningfully, the {PW₉} fragment can be considered to be derived from the reassembly of the {SbW₉} precursor and PO₄ tetrahedron (Figure 2a–c): one corner-sharing W₂O₁₁ group

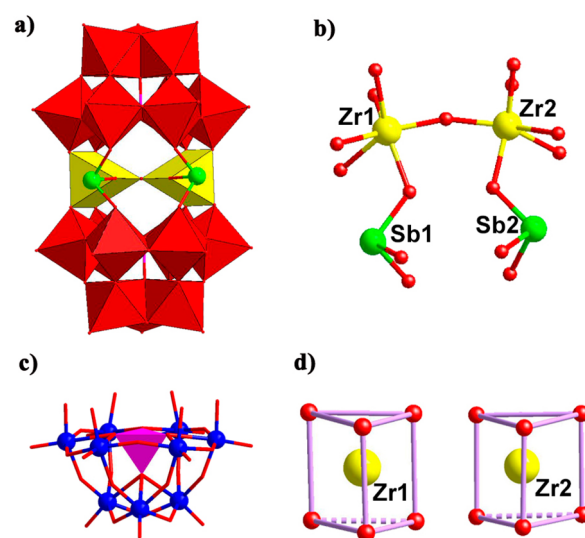


Figure 1. (a) The polyoxoanion of 1. (b) The tetranuclear heterometallic [Zr₂Sb₂O₃]⁸⁺ unit. (c) The {PW₉} fragment. (d) The hexa-coordinate geometry of Zr1⁴⁺ and Zr2⁴⁺.

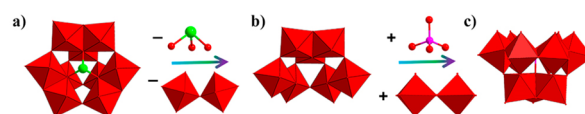


Figure 2. (a) The {SbW₉} precursor. (b) The W₇O₂₈ intermediate. (c) The trivacant Keggin {PW₉} fragment.

and SbO₃ unit are removed from the {SbW₉} precursor to create a W₇O₂₈ intermediate that is then linked to one edge-

sharing W_2O_{10} group via 4 μ -O atoms; a PO_4 tetrahedron occupies the center vacancy of the W_7O_{28} intermediate via 1 μ_4 -O and 3 μ_3 -O atoms, consequently forming the $\{PW_9\}$ fragment.

Different from **1**, **2** crystallizes in the monoclinic space group $P2_1/n$ (Table 1) and contains a polyoxoanion $[ZrSb_4(OH)O_2(A-\alpha-PW_8O_{32})(A-\alpha-PW_9O_{34})]_2^{8-}$ (**2a**, Figure 3a), 6 $[H_2N-$

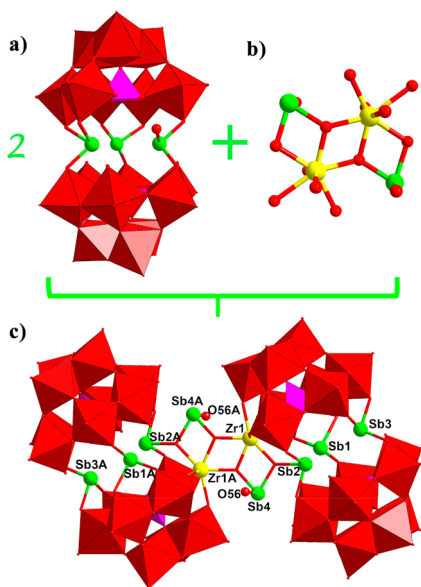


Figure 3. (a) The sandwich-type structure of **2b**. (b) The quadrilateral **2c** fragment. (c) The double sandwich-type representation of **2a**. A: $2 - x, -y, -z$.

$(CH_3)_2]^+$, and 33 lattice water molecules. BVS calculations of **2** indicate that the oxidation states of all the W, P, Sb, and Zr centers are +6, +5, +3 and +4, respectively (Table S2). In addition, the BVS value of the terminal O56 atom connected to Sb4 is 1.08, suggesting that O56 is monoprotonated.

Interestingly, **2a** can be regarded as a double sandwiched configuration, i.e., $\{Sb_2Zr_2\}@\{3Sb\}@\{PW_8\}/\{PW_9\}$, in which $\{PW_9\}$ and $\{PW_8\}$ fragments sandwich 3 Sb^{3+} atoms to form a small-size sandwich-type cluster $\{3Sb\}@\{PW_8\}/\{PW_9\}$ (**2b**), and then, two **2b** are further sandwiched by a $[Sb_2Zr_2(OH)_2O_4]^{4+}$ ($\{Sb_2Zr_2\}$, **2c**) core, resulting in a large-size sandwich-type cluster **2a**. In fact, **2b** is similar to $[Sb_3(SiW_9O_{34})_2]^{11-}$ (**5**),³⁹ but several remarkable differences are as follows: (a) different chemical components of POM fragments, the TP in **2b** (Figure S1a) is dissimilar to the silicotungstate in **5** (Figure S1b); (b) discrepant vacant POM fragments, **2b** contains tri/tetra-vacant $\{PW_9\}/\{PW_8\}$ segments (Figure S1c), whereas there are two identical trivacant $\{SiW_9\}$ in **5** (Figure S1d); (c) distinct linking modes between vacant POM fragments, 3 Sb^{3+} atoms in **2b** connect $\{PW_9\}$ and $\{PW_8\}$ via 8 $Sb-O-W$ linkages, while 9 $Sb-O-W$ linkages exist in **5** joining two $\{SiW_9\}$ fragments. Furthermore, the Zr^{4+} cation in **2c** shows heptacoordinate monocapped trigonal prism geometry (Figure S2). In 2006, Kortz et al. published a dimeric $[Zr_4O_2(OH)_2(H_2O)_4(\beta-SiW_{10}O_{37})_2]^{10-}$ (**6**)⁴⁰ (Figure S3b) where two divacant $[\beta-SiW_{10}O_{37}]^{10-}$ segments sandwiched a $[Zr_4O_2(OH)_2(H_2O)_4]^{10+}$ cluster (Figure S3d). Despite showing similar link modes in tetranuclear metal clusters, the most conspicuous imparities are that **2** is heterometallic and **6** is monometallic. Besides, the

coordination numbers of 3 and 7 for two outer Sb atoms and two inner Zr^{4+} cations in **2c** are distinct from that of 8 and 7 for two outer Zr^{4+} and two inner Zr^{4+} cations in the $[Zr_4O_2(OH)_2(H_2O)_4]^{10+}$ cluster in **6**.

Additionally, the formation of the $\{PW_9\}$ segment in **2** is similar to that in **1**. The $\{PW_8\}$ segment in **2** can also be perceived as a derivative originating from decomposition and reassembly of the $\{SbW_9\}$ precursor: one corner-sharing W_2O_{11} group and heteroatom are taken away from $\{SbW_9\}$ to create the W_7O_{28} intermediate, and then, one WO_6 links to the W_7O_{28} intermediate via 2 μ -O atoms; the PO_4 unit occupies the center vacancy of the W_7O_{28} intermediate via 1 μ_4 -O, 2 μ_3 -O, and 1 μ -O atoms to make the $\{PW_8\}$ segment (Figure S4).

When the pH was increased to 7.5, **3** was surprisingly isolated. Different from **1** and **2**, **3** is a sandwiched TA and crystallizes in the triclinic space group $P\bar{1}$, which contains 8 $[H_2N(CH_3)_2]^+$, 23 Na^+ , 106 lattice water molecules, and two $[Zr_4W_8Sb_4P_5O_{49}(OH)_5(B-\alpha-SbW_9O_{33})_2]^{20-}$ ($\{Zr_4W_8Sb_4P_5\}@\{SbW_9\}_2$, **3a**) polyoxoanions (Figure 4a). BVS calculations

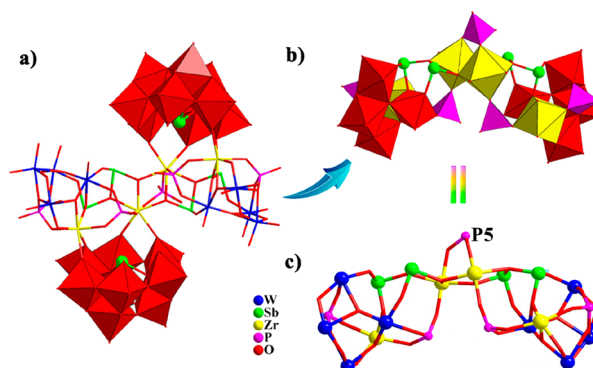


Figure 4. (a) The polyoxoanion **3a**. (b, c) The 21-core $Sb-P-W-Zr$ oxo cluster $[Zr_4W_8Sb_4P_5O_{49}(OH)_5]^{2-}$.

indicate that all the W, Sb, P, and Zr centers are +6, +3, +5, and +4, respectively (Table S3). The terminal oxygens O133, O61, O97, O65, O111, O233, O192, O10, O56, and O231 on P1–P10 are calculated to be 1.39, 1.45, 1.36, 1.25, 1.15, 1.38, 1.23, 1.34, 1.41, and 1.20, respectively, suggesting that they are monoprotonated.

Furthermore, two $\{SbW_9\}$ fragments in **3a** sandwich a unique 21-core cluster $\{Zr_4W_8Sb_4P_5\}$ (**3b**, Figure 4b) via $W-O-Zr$ linkers. Notably, the **3b** cluster contains 4 Zr, 5 P, 4 Sb, and 8 W atoms and can be perceived as the fusion of two $\{ZrW_4Sb_2P_2\}$ units joined by $\{Zr_2P\}$ via $Zr-O-P/Sb$ linkers (Figure 4c). All Zr^{4+} cations are heptacoordinate and exhibit distorted monocapped trigonal prism geometry (Figure S5). Moreover, the **3b** cluster includes two W_4O_{18} ($\{W_4\}$) fragments from the decomposition of the precursors. So far, similar $\{W_4\}$ fragments have been covered in a 20-Ni substituted POT.^{41,42} The $[Ni(enMe)_2]_3[H_6Ni_{20}P_4W_{34}(OH)_4O_{136}(enMe)_8(H_2O)_6]\cdot 12H_2O$ (**7**) contains a W_4O_{16} fragment that somewhat resembles $\{W_4\}$ in the **3b** cluster (Figure 4b). However, apart from different number of O atoms, the distribution motifs of four W atoms in the tetra-W fragment are distinguishing. In **3b**, four W atoms display a tilted trigonal pyramid geometry by standing on four vertexes (Figure S6a,c), which differs from the parallelogram geometry in **7** (Figure S6b,d). Furthermore, the P/Sb atoms in **3b** simultaneously act as bridging atoms. Four tricoordinate Sb

atoms without any terminal O atom are divided into two groups of Sb_2O_5 units. Except for the P5 atom containing two terminal O atoms, the other 4 P atoms have only one terminal O atom, respectively.

Catalytic Oxidation. Since the oxygenation products (sulfoxides and sulfones) of sulfides own multiple applications in the fields of synthetic chemistry, functional materials, and biomedicine, the selective oxidation of sulfides has attracted a widespread and lasting attention.^{43,44} The POMs due to their unique chemical nature (redox properties, flexible acidity, high stability, etc.) are widely accepted as a good candidate for catalysis.^{45,46} Potential application prospects derive us to explore the catalytic performance, and here, **3** has been investigated as a heterogeneous catalyst for catalytic oxidation of various aromatic thioethers by using H_2O_2 oxidant in the acetonitrile solvent (Scheme S1). When one used GC-MS to estimate the catalytic products, the selectivity of sulfoxide and sulfone as well as the conversion of thioethers were quantified by GC (Figure S8).

Our group has reported a Zr_{24} -containing POM as the catalyst to catalyze organic thioethers to sulfones and sulfoxides. Referring to previous catalytic conditions, we first conducted the parallel tests of methylphenyl sulfide (MPS) as a substrate, under the conditions of 0.5 mmol of substrate, 3 O/S molar ratio, 100 S/C molar ratio, 3 mL of acetonitrile, 60 °C, and a 1 h reaction time. It is easy to see from Figure 5 that,

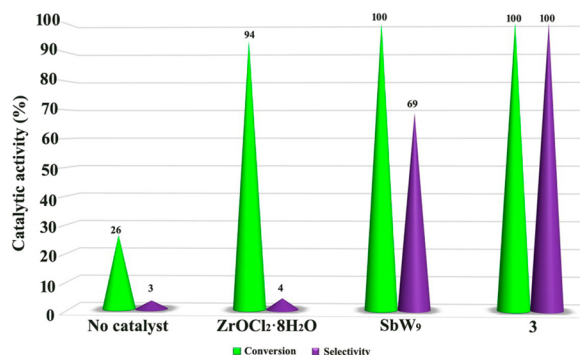


Figure 5. Conversion of MPS and the selectivity of MPSO_2 with different catalysts.

when there is no catalyst, the conversion of MPS is 26%, and the selectivity of the methyl phenyl sulfone (MPSO_2) is 3%; when $\text{ZrOCl}_2 \cdot 8\text{H}_2\text{O}$ and $\{\text{SbW}_9\}$ are the catalysts, the conversion of MPS is 94% and 100%, and the selectivity of MPSO_2 is 4% and 69%. However, when **3** is the catalyst, both the conversion of MPS and the selectivity of MPSO_2 are 100%, indicating **3** possesses a desirable performance.

The explorations of the amount of **3** as catalyst are shown in Figure 6; the conversion of MPS and the selectivity of MPSO_2 are not attenuated as the catalyst dosage decreases within a certain range (100% conversion, 100% selectivity). Therefore, 1000 S/C is adopted to reduce cost.

Additionally, the correlation of the amount of oxidant has been studied at various O/S molar ratios of 1.0, 2.0, 2.2, 2.4, 2.6, 2.8, and 3.0. Theoretically, the catalytic oxidation has a complete reaction when the O/S is 2 under the premise that the effective utilization rate of the oxidant is 100%, but it may be difficult to achieve due to some unavoidable factors such as partial decomposition of H_2O_2 during the reaction. As shown in Figure 7, when the O/S is 2.2, almost all MPS completely

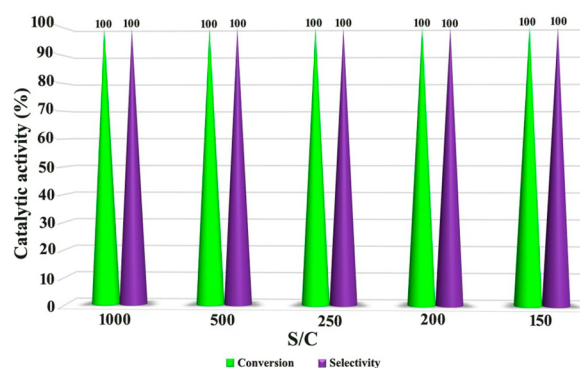


Figure 6. Conversion of MPS and the selectivity of MPSO_2 with different amounts of catalyst **3**.

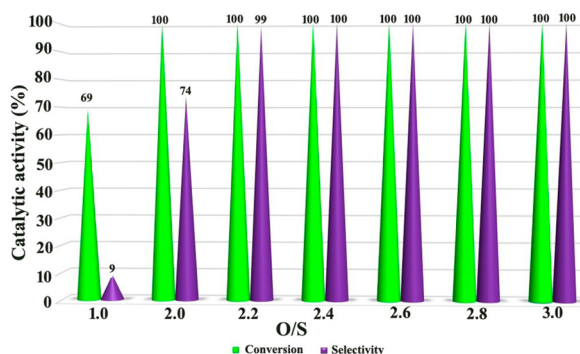


Figure 7. Conversion of MPS and the selectivity of MPSO_2 at different amounts of oxidizer.

converts to MPSO_2 and the efficiency of H_2O_2 also reaches over 90%. While the O/S of 2.4 leads to 100% conversion of MPS and 100% selectivity of MPSO_2 , exhibiting more excellent catalytic performance, it was chosen for the following experiments.

The reaction temperature and time are significant criteria for evaluating catalysts in the catalytic oxidation process. The results of the parallel experiments reveal that the conversion of MPS and the selectivity of MPSO_2 are both 100% at the relatively mild 45 °C, which is superior to that of the Zr_{24} -catalyzed oxidation of thioethers previously reported; hence, 45 °C is selected for the optimal experimental temperature (Figure 8). Additionally, we have attempted to shorten the reaction time to 30 min, but the selectivity of MPSO_2 is greatly reduced; so, 60 min is still the choice (Figure 9).

Furthermore, the cyclic experiments have been conducted for MPS to evaluate the catalyst performance of **3** under the optimal conditions. In the heterogeneous catalytic cycle experiments, the catalyst at the end of each experiment was collected by filtration and then reused for the next test. As shown in Figure 10, the conversion and selectivity are 100% in the first three cycles, and in the next two cycles, **3** still maintains excellent performance with the conversion of 100% in spite of a slight reduction of the selectivity. Moreover, the catalytic oxidation of diphenyl sulfide (DPS) has also been systematically studied while keeping other conditions constant (Figures S9–S12). Obviously, temperature is more vital than catalytic time during the catalytic oxidation of DPS. At 45 °C for 60 min, 100% conversion and 89% selectivity are obtained. However, at 60 °C, 100% conversion and 96% selectivity can be achieved in only 15 min. Besides, under the optimal

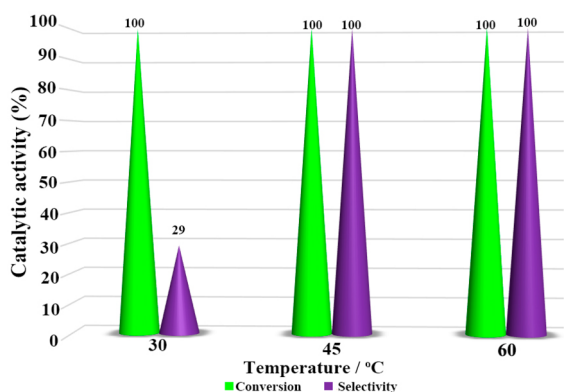


Figure 8. Conversion of MPS and the selectivity of MPSO₂ at different reaction temperatures.

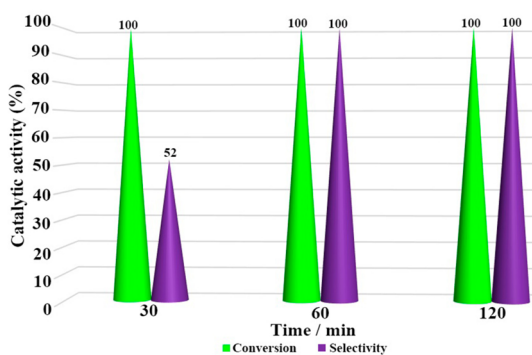


Figure 9. Conversion of MPS and the selectivity of MPSO₂ at different reaction times.

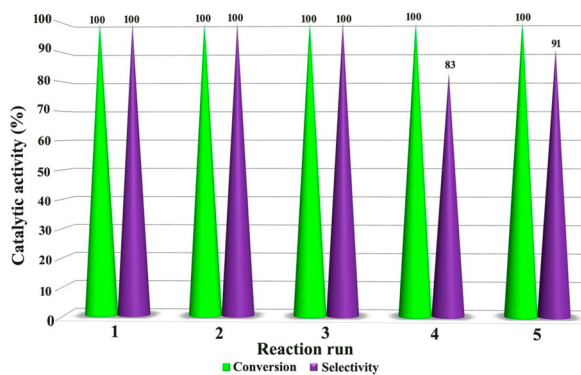
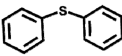
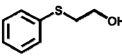
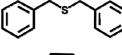
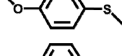
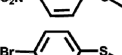
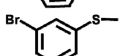
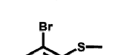
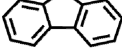
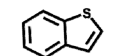


Figure 10. Recycling of the catalytic system for the oxidation of MPS at 45 °C and 2.4 O/S.

conditions, the results of the cycle experiments for DPS also demonstrate the excellent catalytic performance of 3. In addition, the stability of 3 was determined by comparing the PXRD patterns and IR spectra before and after the catalytic reaction (Figure S13).

Moreover, the conversion and selectivity of most tested aromatic thioethers are higher than 98% (Table 2, entries 1, 3–8) under the following conditions: 0.5 mmol of substrate, 2.4 O/S, 1000 S/C, 3 mL of acetonitrile, 45 °C, and 1 h. The conversion and selectivity of 2-bromothioanisole, benzothiophene, and dibenzothiophene, which are generally extremely difficult to catalyze oxidation, are enhanced by increasing temperature and prolonging reaction time (entry 9–11). When the temperature is elevated from 45 to 60 °C, the selectivity of

Table 2. Selective Oxidation of Various Aromatic Thioethers to Sulfones

Entry	Substrate	Time (h)	Temp. (°C)	Cov. (%)	Selectivity (%)	RR'SO/RR'SO ₂
1		1	45	100	0	100
2		1	45	100	11	89
		0.5	60	100	0	100
3		1	45	100	0	100
4		1	45	100	0	100
5		1	45	98	0	100
6		1	45	100	0	100
7		1	45	100	0	100
8		1	45	100	0	100
9		1	45	100	82	18
		1	60	100	61	39
10		1	60	100	0	100
		1	60	48	7	93
11		1	60	64	1	99
		2	60	64	1	99

2-bromophenyl methyl sulfone can be promoted from 18% to 39% (entry 9). Besides, at 60 °C, we obtain an extremely desirable result for the catalytic oxidation of dibenzothiophene (entry 10), while the conversion of benzothiophene is still relatively low at 60 °C. Sequentially, when the reaction time is extended from 1 to 2 h, the conversion of benzothiophene is improved from 48% to 64% and the selectivity increases from 93% to 99% (entry 11).

CONCLUSIONS

In summary, three novel Zr-substituted POT aggregates have been made under hydrothermal reactions. 1 is a mono-sandwich-type dimer $\{Zr_2Sb_2\}@(\{PW_9\})_2$, while 2 is a double sandwiched structure, in which the small-size sandwiched $\{3Sb\}@(\{PW_8\}\{PW_9\})$ cluster contains two different fragments of $\{PW_8\}$ and $\{PW_9\}$, and two such sandwich-type units are further sandwiched by one $\{Sb_2Zr_2\}$ core to form a novel large-size sandwich-type cluster aggregate $\{Sb_2Zr_2\}@[\{3Sb\}@(\{PW_8\}\{PW_9\})]_2$. 3 is a double cluster aggregate, in which each aggregate contains two $\{SbW_9\}$ fragments and one unique 21-core $\{Zr_4W_8Sb_4P_5\}$ cluster: two $\{SbW_9\}$ fragments are further sandwiched by one 21-core $\{Zr_4W_8Sb_4P_5\}$ cluster to produce a sandwich-type $\{Zr_4W_8Sb_4P_5\}@(\{SbW_9\})_2$ cluster aggregate. The thermal stability of 3 has been investigated by recording infrared spectra at different temperatures, suggesting that 3 is stable to 350 °C. Furthermore, the catalytic oxidation of thioethers by 3 as the heterogeneous catalyst has been explored in detail, showing that 3 possesses high conversion and remarkable selectivity in the catalytic oxidation of aromatic thioethers with H₂O₂ and exhibits excellent recyclability.

■ ASSOCIATED CONTENT

SI Supporting Information

The Supporting Information is available free of charge at <https://pubs.acs.org/doi/10.1021/acs.inorgchem.0c01910>.

BVS calculations of W, Zr, P, and Sb atoms in 1–3; related structural figures; IR spectra; TG curves of 1–3 (PDF)

Accession Codes

CCDC 1882473–1882475 contain the supplementary crystallographic data for this paper. These data can be obtained free of charge via www.ccdc.cam.ac.uk/data_request/cif, or by emailing data_request@ccdc.cam.ac.uk, or by contacting The Cambridge Crystallographic Data Centre, 12 Union Road, Cambridge CB2 1EZ, UK; fax: +44 1223 336033.

■ AUTHOR INFORMATION

Corresponding Author

Guo-Yu Yang – MOE Key Laboratory of Cluster Science, School of Chemistry and Chemical Engineering, Beijing Institute of Technology, Beijing 102488, China; orcid.org/0000-0002-0911-2805; Email: yyg@bit.edu.cn

Authors

Hai-Lou Li – MOE Key Laboratory of Cluster Science, School of Chemistry and Chemical Engineering, Beijing Institute of Technology, Beijing 102488, China

Chen Lian – MOE Key Laboratory of Cluster Science, School of Chemistry and Chemical Engineering, Beijing Institute of Technology, Beijing 102488, China

Da-Peng Yin – MOE Key Laboratory of Cluster Science, School of Chemistry and Chemical Engineering, Beijing Institute of Technology, Beijing 102488, China

Complete contact information is available at: <https://pubs.acs.org/10.1021/acs.inorgchem.0c01910>

Notes

The authors declare no competing financial interest.

■ ACKNOWLEDGMENTS

This work was supported by the NSFC (nos. 21831001, 21571016, and 91122028) and the NSFC for Distinguished Young scholars (no. 20725101).

■ REFERENCES

- (1) Marrot, J.; Pilette, M. A.; Haouas, M.; Floquet, S.; Taulelle, F.; López, X.; Poblet, J. M.; Cadot, E. Polyoxometalates paneling through {Mo₂O₂S₂} coordination: cation-directed conformations and chemistry of a supramolecular hexameric scaffold. *J. Am. Chem. Soc.* **2012**, *134*, 1724–1737.
- (2) Heine, J.; Müller-Buschbaum, K. Engineering metal-based luminescence in coordination polymers and metal-organic frameworks. *Chem. Soc. Rev.* **2013**, *42*, 9232–9242.
- (3) Zheng, S.-T.; Zhang, J.; Li, X.-X.; Fang, W.-H.; Yang, G.-Y. Cubic polyoxometalate-organic molecular cage. *J. Am. Chem. Soc.* **2010**, *132*, 15102–15103.
- (4) Li, H.-L.; Lian, C.; Chen, L.-J.; Zhao, J.-W.; Yang, G.-Y. Two Ce³⁺-Substituted Selenotungstates Regulated by N,N-Dimethyl ethanolamine and Dimethylamine Hydrochloride. *Inorg. Chem.* **2019**, *58*, 8442–8450.
- (5) Keggin, J. F. Structure of the Molecule of 12-Phosphotungstic Acid. *Nature* **1933**, *131*, 908–909.
- (6) Rhule, J. T.; Hill, C. L.; Judd, D. A.; Schinazi, R. F. Polyoxometalates in medicine. *Chem. Rev.* **1998**, *98*, 327–358.

- (7) Proust, A.; Matt, B.; Villanneau, R.; Guillemot, G.; Gouzerh, P.; Izzet, G. Functionalization and post-functionalization: a step towards polyoxo-metalate-based materials. *Chem. Soc. Rev.* **2012**, *41*, 7605–7622.

- (8) Miras, H. N.; Yan, J.; Long, D. L.; Cronin, L. Engineering polyoxo-metalates with emergent properties. *Chem. Soc. Rev.* **2012**, *41*, 7403–7430.

- (9) Li, H.-L.; Liu, Y.-J.; Liu, J.-L.; Chen, L.-J.; Zhao, J.-W.; Yang, G.-Y. Structural transformation from dimerization to tetramerization of serine-decorated rare-earth-incorporated arsenotungstates induced by the usage of rare-earth salts. *Chem. - Eur. J.* **2017**, *23*, 2673–2689.

- (10) Ma, P. T.; Hu, F.; Wan, R.; Huo, Y.; Zhang, D. D.; Niu, J. Y.; Wang, J. P. Magnetic double-tartaric bridging mono-lanthanide substituted phospho-tungstates with photochromic and switchable luminescence properties. *J. Mater. Chem. C* **2016**, *4*, 5424–5433.

- (11) Li, H.-L.; Liu, Y.-J.; Li, Y.-M.; Chen, L.-J.; Zhao, J.-W.; Yang, G.-Y. Unprecedented selenium and lanthanide simultaneously bridging seleno-tungstate aggregates stabilized by four tetra-vacant Dawson-like {Se₂W₁₄} units. *Chem. - Asian J.* **2018**, *13*, 2897–2907.

- (12) Zheng, S.-T.; Zhang, J.; Yang, G.-Y. Designed synthesis of POM-organic frameworks from {Ni₆PW₉} building blocks under hydrothermal conditions. *Angew. Chem., Int. Ed.* **2008**, *47*, 3909–3913.

- (13) Zhao, J.-W.; Zhang, J.; Zheng, S.-T.; Yang, G.-Y. Combination of lacunary polyoxometalates and high-nuclear transition-metal clusters under hydrothermal conditions. 5. A novel tetrameric cluster of [Fe^{II}Fe^{III}₁₂(μ₃-OH)₁₂(μ₄-PO₄)₄}(B-α-PW₉O₃₄)₄]²²⁻. *Inorg. Chem.* **2007**, *46*, 10944–10946.

- (14) Clemente-Juan, J. M.; Coronado, E.; Forment-Aliaga, A.; Galán-Mascarós, J. R.; Giménez-Saiz, C.; Gómez-García, C. J. A new hepta-nuclear cobalt(II) cluster encapsulated in a novel hetero-polyoxometalate topology: synthesis, structure, and magnetic properties of [Co₇(H₂O)₂(OH)₂P₂W₂₅O₉₄]¹⁶⁻. *Inorg. Chem.* **2004**, *43*, 2689–2694.

- (15) Ibrahim, M.; Lan, Y. H.; Bassil, B. S.; Xiang, Y. X.; Suchopar, A.; Powell, A. K.; Kortz, U. Hexadecacobalt(II)-containing polyoxometalate-based single-molecule magnet. *Angew. Chem., Int. Ed.* **2011**, *50*, 4708–4711.

- (16) Goberna-Ferron, S.; Vigara, L.; Soriano-Lopez, J.; Galán-Mascarós, J. R. Identification of a nonanuclear {Co^{II}₉} polyoxometalate cluster as a homogeneous catalyst for water oxidation. *Inorg. Chem.* **2012**, *51*, 11707–11715.

- (17) Li, B.; Zhao, J.-W.; Zheng, S.-T.; Yang, G.-Y. Combination chemistry of hexa-copper-substituted polyoxometalates driven by the Cu^{II}-polyhedra distortion: from tetramer, 1D chain to 3D framework. *Inorg. Chem.* **2009**, *48*, 8294–8303.

- (18) Zhang, Z.-M.; Duan, X. P.; Yao, S.; Wang, Z. S.; Lin, Z. K.; Li, Y.-G.; Long, L.-S.; Wang, E.-B.; Lin, W. B. Cation-mediated optical resolution and anticancer activity of chiral polyoxometalates built from entirely achiral building blocks. *Chem. Sci.* **2016**, *7*, 4220–4229.

- (19) Artetxe, B.; Reinoso, S.; Felices, L. S.; Vitoria, P.; Pache, A.; Martín-Caballero, J.; Gutierrez-Zorrilla, J. M. Functionalization of Krebs-Type Polyoxometalates with N,O-Chelating Ligands: A Systematic Study. *Inorg. Chem.* **2015**, *54*, 241–252.

- (20) Cai, Z.-W.; Yang, T.; Qi, Y.-J.; Li, X.-X.; Zheng, S.-T. A temperature-resolved assembly of a series of the largest scandium-containing polyoxotungstates. *Dalton Trans.* **2017**, *46*, 6848–6852.

- (21) Huang, L.; Wang, S.-S.; Zhao, J.-W.; Cheng, L.; Yang, G.-Y. Synergistic combination of multi-Zr^{IV} cations and lacunary Keggin germanotungstates leading to a gigantic Zr₂₄-cluster-substituted polyoxometalate. *J. Am. Chem. Soc.* **2014**, *136*, 7637–7642.

- (22) Kikukawa, Y.; Yamaguchi, S.; Tsuchida, K.; Nakagawa, Y.; Uehara, K.; Yamaguchi, K.; Mizuno, N. Synthesis and catalysis of di- and tetra-nuclear metal sandwich-type silicotungstates [(γ-SiW₁₀O₃₆)₂M₂(μ-OH)₂]¹⁰⁻ and [(γ-SiW₁₀O₃₆)₂M₄(μ₄-O)(μ-OH)₆]⁸⁻ (M = Zr or Hf). *J. Am. Chem. Soc.* **2008**, *130*, 5472–5478.

- (23) Fang, X.-K.; Anderson, T. M.; Hill, C. L. Enantiomerically pure polytungstates: chirality transfer through zirconium coordination

centers to nanosized inorganic clusters. *Angew. Chem., Int. Ed.* **2005**, *44*, 3540–3544.

(24) Fang, X. K.; Anderson, T. M.; Hou, Y.; Hill, C. L. Stereoisomerism in polyoxometalates: structural and spectroscopic studies of bis(malate)-functionalized cluster systems. *Chem. Commun.* **2005**, 5044–5046.

(25) Bassil, B. S.; Dickman, M. H.; Kortz, U. Synthesis and Structure of Asymmetric Zirconium-Substituted Silicotungstates, $[\text{Zr}_6\text{O}_2(\text{OH})_4(\text{H}_2\text{O})_3(\beta\text{-SiW}_{10}\text{O}_{37})_3]^{14-}$ and $[\text{Zr}_4\text{O}_2(\text{OH})_2(\text{H}_2\text{O})_4(\beta\text{-SiW}_{10}\text{O}_{37})_2]^{10-}$. *Inorg. Chem.* **2006**, *45*, 2394–2396.

(26) Al-Kadamany, G.; Mal, S. S.; Milev, B.; Donoeva, B. G.; Maksimovsk-Aya, R. I.; Kholdeeva, O. A.; Kortz, U. Hexazirconium- and hexahafnium-containing tungstoarsenates (III) and their oxidation catalysis properties. *Chem. - Eur. J.* **2010**, *16*, 11797–11800.

(27) Zhang, Z.; Li, H.-L.; Wang, Y.-L.; Yang, G.-Y. Syntheses, Structures, and Electrochemical Properties of Three New Acetate-Functionalized Zirconium-Substituted Germanotungstates: From Dimer to Tetramer. *Inorg. Chem.* **2019**, *58*, 2372–2378.

(28) Nsouli, N. H.; Ismail, A. H.; Helgadottir, I. S.; Dickman, M. H.; Clemente-Juan, J. M.; Kortz, U. Copper-, Cobalt-, and Manganese-Containing 17-Tungsto-2-Germanates. *Inorg. Chem.* **2009**, *48*, 5884–5890.

(29) Haider, A.; Ibrahim, M.; Bassil, B. S.; Carey, A. M.; Viet, A. N.; Xing, X. L.; Ayass, W. W.; Miñambres, J. F.; Liu, R. L.; Zhang, G. J.; Keita, B.; Mereacre, V.; Powell, A. K.; Balinski, K.; N'Diaye, A. T.; Küpper, K.; Chen, H.-Y.; Stimming, U.; Kortz, U. Mixed-Valent Mn_{16} -Containing Heteropolyanions: Tuning of Oxidation State and Associated Physicochemical Properties. *Inorg. Chem.* **2016**, *55*, 2755–2764.

(30) Li, H.-L.; Liu, Y.-J.; Zheng, R.; Chen, L.-J.; Zhao, J.-W.; Yang, G.-Y. Trigonal pyramidal $\{\text{AsO}_2(\text{OH})\}$ bridging tetranuclear rare-earth encapsulated polyoxotungstate aggregates. *Inorg. Chem.* **2016**, *55*, 3881–3893.

(31) Chen, W.-C.; Qin, C.; Li, Y.-G.; Zang, H.-Y.; Shao, K.-Z.; Su, Z.-M.; Wang, E.-B.; Liu, H.-S. Assembly of tetrameric dimethyltin-functionalized selenotungstates: from nanoclusters to one-dimensional chains. *Chem. Commun.* **2015**, *51*, 2433–2436.

(32) Wang, J. P.; Ma, P. T.; Shen, Y.; Niu, J. Y. A novel polyoxotungstate $[\text{Ni}_4(\text{H}_2\text{O})_2(\alpha\text{-NiW}_9\text{O}_{34})_2]^{16-}$ based on an old structure with a new component. *Cryst. Growth Des.* **2007**, *7*, 603–605.

(33) Cai, J.; Zheng, X.-Y.; Xie, J.; Yan, Z.-H.; Kong, X.-J.; Ren, Y. P.; Long, L.-S.; Zheng, L.-S. Anion-dependent assembly of heterometallic 3d-4f clusters based on a lacunary polyoxometalate. *Inorg. Chem.* **2017**, *56*, 8439–8445.

(34) Zhang, D. D.; Wang, C. Z.; Li, S. Z.; Liu, J. P.; Ma, P. T.; Wang, J. P.; Niu, J. Y. Syntheses, characterization and magnetic properties of two novel inorganic-organic tungstoferrites, $[\text{Fe}^{\text{III}}_4(\text{H}_2\text{O})_2(\text{B-a-Fe}^{\text{III}}\text{W}_9\text{O}_{34})_2]^{10-}$. *J. Solid State Chem.* **2013**, *198*, 18–23.

(35) Wang, Z.-S.; Zhang, Z.-M.; Han, X.-B.; Zhang, H.; Wang, E.-B. Extended structure constructed from organic ligands functionalized-sandwich-type tungstoferrates. *Inorg. Chem. Commun.* **2012**, *20*, 196–200.

(36) Li, H.-L.; Zhang, Z.; Wang, Y.-L.; Yang, G.-Y. A Trinuclear Zr-substituted decanuclear hetero-metal sandwich tungstoantimonate: synthesis, Structure and properties. *Eur. J. Inorg. Chem.* **2019**, 2019, 486–491.

(37) Li, H.-L.; Wang, Y.-L.; Zhang, Z.; Yang, B.-F.; Yang, G.-Y. A new tetra-Zr(IV)-substituted polyoxotungstate aggregate. *Dalton Trans.* **2018**, *47*, 14017–14024.

(38) Brown, I. D.; Altermatt, D. Bond-valence parameters obtained from a systematic analysis of the inorganic crystal structure database. *Acta Crystallogr., Sect. B: Struct. Sci.* **1985**, *B41*, 244–247.

(39) Assran, A. S.; Izarova, N. V.; Banerjee, A.; Rabie, U. M.; Abou-El-Wafab, M. H. M.; Kortz, U. The antimony(III)-bridged heteropolyanion sandwich dimers $[\text{Sb}^{\text{III}}_3(\text{A-}\alpha\text{-XW}_9\text{O}_{34})_2]^{11-}$ ($\text{X} = \text{Si}^{\text{IV}}, \text{Ge}^{\text{IV}}$) and C-shaped double-sandwich $[\text{Sb}^{\text{III}}_6\text{O}_2(\text{PW}_6\text{O}_{26})(\text{A-}\alpha\text{-PW}_9\text{O}_{34})_2]^{15-}$. *Dalton Trans.* **2012**, *41*, 9914–9921.

(40) Bassil, B. S.; Dickman, M. H.; Kortz, U. Synthesis and structure of asymmetric zirconium-substituted silicotungstates, $[\text{Zr}_6\text{O}_2(\text{OH})_4(\text{H}_2\text{O})_3(\beta\text{-SiW}_{10}\text{O}_{37})_3]^{14-}$ and $[\text{Zr}_4\text{O}_2(\text{OH})_2(\text{H}_2\text{O})_4(\beta\text{-SiW}_{10}\text{O}_{37})_2]^{10-}$. *Inorg. Chem.* **2006**, *45*, 2394–2396.

(41) Zheng, S.-T.; Zhang, J.; Clemente-Juan, J. M.; Yuan, D.-Q.; Yang, G.-Y. Poly (polyoxotungstate) s with 20 nickel centers: from nanoclusters to one-dimensional chains. *Angew. Chem., Int. Ed.* **2009**, *48*, 7176–7179.

(42) Zhao, J. W.; Shi, D. Y.; Chen, L. J.; Ma, P. T.; Wang, J. P.; Niu, J. Y. Two 1-D multi-nickel substituted arsenotungstate aggregates. *CrystEngComm* **2011**, *13*, 3462–3469.

(43) Uematsu, T.; Miyamoto, Y.; Ogasawara, Y.; Suzuki, K.; Yamaguchi, K.; Mizuno, N. Molybdenum-doped $\alpha\text{-MnO}_2$ as an efficient reusable heterogeneous catalyst for aerobic sulfide oxygenation. *Catal. Sci. Technol.* **2016**, *6*, 222–233.

(44) Fernández, I.; Khiar, N. Recent Developments in the Synthesis and Utilization of Chiral Sulfoxides. *Chem. Rev.* **2003**, *103*, 3651–3706.

(45) Wang, S.-S.; Yang, G.-Y. Recent Advances in polyoxometalate-catalyzed reactions. *Chem. Rev.* **2015**, *115*, 4893–4962.

(46) Li, H.-L.; Lian, C.; Yin, D.-P.; Jia, Z.-Y.; Yang, G.-Y. A new hepta-nuclear Ti-oxo-cluster-substituted tungstoantimonate and its catalytic oxidation of thioethers. *Cryst. Growth Des.* **2019**, *19*, 376–380.